Journal of Power Sources 189 (2009) 660–664

Contents lists available at ScienceDirect

Journal of Power Sources

journal homepage: www.elsevier.com/locate/jpowsour

Short communication

Studies of interfacial reactions on thin film electrodes of Sn during initial cycling using infrared spectroscopy

S.-W. Baek[a], S.-J. Hong[a], D.-W. Kim[b], S.-W. Song[a,*]

[a] Department of Fine Chemical Engineering & Applied Chemistry, Chungnam National University, Daejeon 305-764, South Korea
[b] Department of Chemical Engineering, Hanyang University, Seoul 133-791, South Korea

ARTICLE INFO

Article history:
Received 2 September 2008
Accepted 8 September 2008
Available online 19 September 2008

Keywords:
Interfacial reaction
Sn
Initial cycling
Ex-situ ATR FTIR

ABSTRACT

Interfacial reactions of Sn during initial cycling in 1 M $LiPF_6$/EC:DMC (1:1) were studied by characterizing the surface species formed on thin film electrodes of Sn, prepared with a pulsed laser deposition, using *ex-situ* ATR FTIR spectroscopy and microscopy. FTIR analyses indicated that at high voltage region above 1.0 V vs. Li/Li^+ the surface of Sn electrode was covered by PF-containing inorganic species probably by the interfacial reactions between Sn and PF_6^- anions. With charging to 0.63 V low amounted organic species with carboxylate metal salt and alkyl functionalities appeared, due to the reductive decomposition of organic solvents. The organic surface species however were destroyed upon a deep charge to 0.1 V and reproduced on the subsequent discharge process, whereas P–F containing inorganic species remained preserved. No sustainment of organic surface species but the stable passivation of Sn surface by PF-containing species during initial cycling are believed to cause unstable interfacial structure and the possibility of reduced utilization of active Sn, respectively, resulting in the large initial irreversible capacity loss.

1. Introduction

Sn-based intermetallics and carbon composites have been of interest for use as alternative anode materials in lithium batteries, but have shown a rapid capacity decline in the initial ten cycles [1,2]. Long term cyclability and rate capability of lithium cells with Sn-based anode materials were suggested to be mainly limited by large structural volume change followed by particle pulverization and the loss of particles contact occurring during alloying–dealloying cycles. Recently we obtained an experimental clue of another cause responsible for the capacity decline, which is originated from the Sn electrode–electrolyte interfacial reactions that is somewhat different from graphite. Also the concentration of surface species formed by interfacial reactions of Sn was found to increase with cycling. Recollecting that lithium ion transport should begin to occur at the electrode–electrolyte interface, structural volume change and particle pulverization that certainly occur with changes in active surface area might correlate to the interfacial reaction of Sn with electrolyte and initial cycling behavior. Chiu et al. [3] and Inaba et al. [4] reported that the solid electrolyte interface (SEI) layer formed mainly above 1.0 V vs. Li/Li^+, which is a bit higher than that for graphite (ca. 0.7–1.0 V). Beattie et al. [5] predicted that high voltage (>1.5 V) irreversible capacity loss of Sn film electrode was related to the catalytic reaction of clean Sn metal with electrolyte. However, what interfacial reactions occur at such high voltage region and the other possible reaction at lower voltage region are not currently understood.

Understanding of the interfacial reaction behavior, in particular, during the early stage of cycling and the clarification of the cause for rapid initial capacity decline are extremely crucial, since the performance over next cycles is often controlled by initial interfacial reactions. It is thus necessary to determine the surface species formed at different voltage region during the operation of a lithium cell and to establish surface chemistry occurring on Sn. In that way, the paths stabilizing Sn electrode–electrolyte interfacial structure can be figured out. However, the complications from carbon and binder additives that are included in the bulk electrodes can obstruct the precise investigation of interfacial reactions. Studies with thin film electrodes deposited on electronically conductive substrate with pulsed laser deposition can give clearer insights into the surface chemistry [6–8] without the complications from additives. For film surface characterization, we focused on *ex-situ* attenuated total reflectance (ATR) FTIR analysis, which is very sensitive to surface species [9] and provides direct information on the functional groups of surface molecules, compatible with other surface analyses results (e.g. X-ray photoelectron spectroscopy) [10,11]. Even though *in-situ* IR analysis can provide real time observation of interfacial reactions, the IR features of electrolyte

* Corresponding author. Tel.: +82 42 821 7008 fax: +82 42 822 6637.
E-mail address: swsong@cnu.ac.kr (S.-W. Song).

0378-7753/$ – see front matter © 2008 Elsevier B.V. All rights reserved.
doi:10.1016/j.jpowsour.2008.09.035

components often overlap with the signals from SEI layer composition, which makes the characterization of the SEI layer extremely difficult. Instead, *ex-situ* IR spectral measurement on thin film electrode with attenuated total reflection (ATR) technique can provide higher quality spectra and precise surface characterization of the SEI layer on battery electrodes [12–14].

Here we report *ex-situ* ATR FTIR spectroscopic and microscopic characterization of the surface species formed on the Sn thin film electrode during initial cycling. Possible initial interfacial reactions and their influences on cyclability of Sn electrode are estimated.

2. Experimental

The 58 nm thick films of Sn were prepared on stainless steel (SS) substrates with a pulsed laser deposition (PLD) at room temperature with 2 min deposition in 5 mTorr of Ar, as described elsewhere [8]. As-deposited film was 58 nm thick, determined using FESEM, and crystallized in the tetragonal (*I41/amd*) structure of Sn (JCPDS No. 86–2264), evaluated using XRD analysis. The electrochemical cell, containing the Sn/SS electrode as a working electrode with a Li reference electrode and a Li counter electrode, has been used. Cell assembly and testing were conducted in the Ar-filled glove box with the water and oxygen contents of about 1 ppm. The state of charge (SOC) of the film was controlled by charging (cathodic) a lithium cell at a current density of 35 $\mu A\,cm^{-2}$ to the given cut-off voltages in the electrolyte of 1 M $LiPF_6$ in ethylene carbonate (EC) and dimethyl carbonate (DMC) with 1:1 volume ratio (Techno Semichem) with about 3 ppm level of water, followed by holding at those voltages for a while, using galvanostat (CHI 660). A cell cut off at 0.7 V showed a rapid drop of its OCV to 0.63 V, thus, this cell will be called as charged to 0.63 V henceforth.

The films were separated from the cells, washed with DMC (Techno Semichem) for 20 s followed by drying at room temperature in the glove box and subjected to FTIR measurement using IR spectrometer (Bruker optics IFS66 V/S) equipped with a MCT detector. The FTIR spectra were acquired in the single reflection ATR using a Ge optic. Prior to the FTIR measurements, charged and cycled films were directly mounted on the tightly sealed ATR unit in the Ar-filled glove box to avoid exposure to air. Spectral resolution was 4 cm^{-1} and total 512 scans were co-added. Surface morphology of Sn/SS films after charging and cycling was obtained using a field emission SEM (Jeol JSM-7000F) at 10 kV. To minimize exposure to air, all films were mounted on the SEM holder in the Ar-filled glove box, placed in a portable vacuum carrier and moved to SEM vacuum chamber.

3. Results and discussion

3.1. Constant current cycling

First charge–discharge voltage profile of a lithium cell with Sn/SS film electrode in the region of 0.1–1.0 V is shown in Fig. 1a. The OCV was 2.38 V attributed to surface tin oxide impurities probably formed during film preparation. First charge and discharge specific capacities of Sn/SS electrode were 1730 and 554 mA h g^{-1}, respectively, with a low efficiency of 32%, calculated based on the weight of the film, which was estimated from the measured thickness, the area of the electrode and the crystallographic density 7.29 gcm^{-3} of Sn. The initial charge capacity value exceeds the value of the stoichiometric lithiation mechanism, which are about 990 mA h g^{-1} for $Li_{4.4}Sn$. Error (ca. 10–20%) can be from the usage of the theoretical density of Sn or film thickness evaluation for gravimetric capacity calculation. Also the presence of surface tin oxide may contribute to the initial charge capacity above 1.0 V,

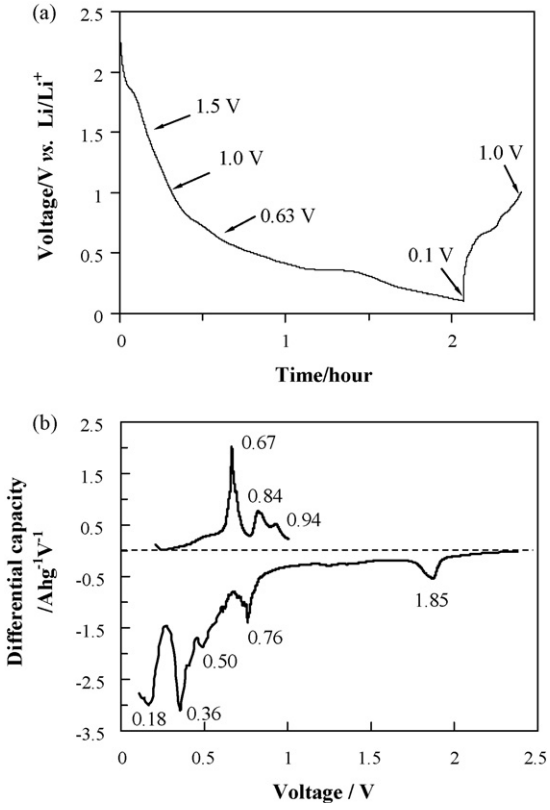

Fig. 1. Voltage profile of a lithium cell with Sn/SS film electrode during initial cycling in the voltage region of 0.1–1.0 V vs. Li/Li^+ (a) and its differential capacity plot (b). Five identical cells were charged to the given cut-off voltages marked with arrows, and cycled between 0.1 and 1.0 V, respectively.

amounted as approximately 300 mA h g^{-1}. The data suggest that the reduction of electrolyte components on the surface of Sn is responsible for the extra charge capacity and the low initial cycling efficiency.

Interfacial reaction behavior of Sn was studied by characterizing the surface species formed on the electrode at various SOC. In order to control the SOC, several identical cells with Sn/SS film electrodes were charged to various cut-off voltages as marked with arrows in Fig. 1a, using constant current at 35 $\mu A\,cm^{-2}$. Because this material is supposed to be an anode in full cells, we define charge as the cathodic addition of Li to Sn (alloying), whereas discharge as the anodic delithiation (dealloying). In the course of alloying and dealloying with lithium, the film exhibits several plateaus in Fig. 1a, in particular, near 0.7 and 0.3 V, due to the phase transitions in Li_xSn with variable lithium content (x). In Fig. 1b, the anodic and cathodic peaks corresponding to the plateaus are better shown in differential capacity plot of the voltage profile. The initial cathodic curve shows a small peak at 1.85 V that is attributable to the reduction of electrolyte and/or the lithiation of surface oxide impurity. The lithiation process is continued by the peaks at 0.76 and 0.50 V, and dominant peaks at 0.36 and 0.18 V, forming from Li_xSn with variable x to $Li_{4.4}Sn$, consistent with earlier reports that the $Li_{4.4}Sn$ forms below 0.4 V during alloying of Sn with lithium, *via* multiphase alloys, Li_xSn with $x = 0.4$–2.3 near 0.5–0.8 V [1,2]. Cathodic contributions in the region of above $\sim$ 0.6 V are also attributable to the reduction of electrolyte components forming a SEI layer. On the reverse process, the three anodic peaks clearly observed at 0.67, 0.84 and 0.94 V may be associated with the regeneration of the $Li_{2.3}Sn$/LiSn, $Li_{0.4}Sn$ and pure Sn phases, respectively [2].

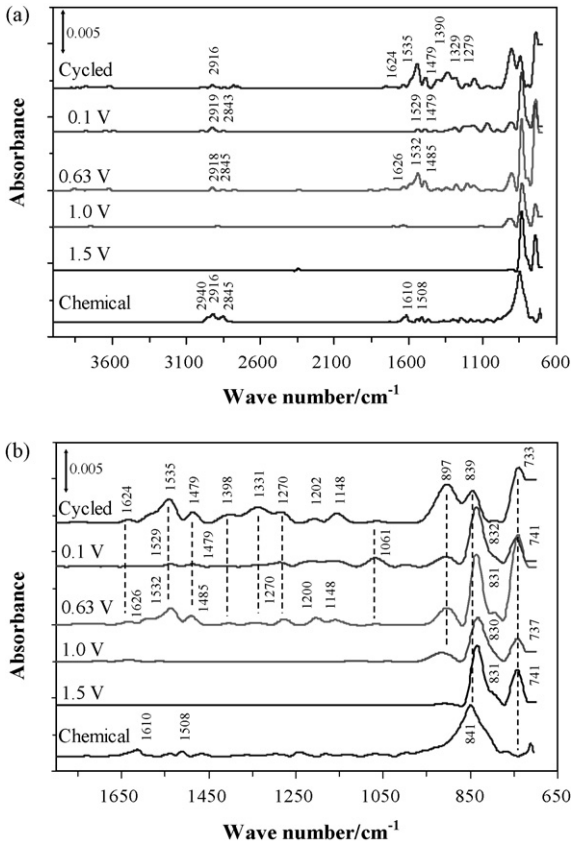

Fig. 2. IR spectra of Sn/SS film electrodes obtained after chemical reaction, and after charging to 1.5, 1.0, 0.63, 0.1 V, and initial cycling between 0.1 and 1.0 V followed by DMC washing and drying (a), and their magnifications in lower frequency region (b).

3.2. FTIR characterization of the surface species after charging and cycling

Fig. 2a and b show the FTIR spectra of the surface of Sn/SS electrode obtained after charging (cathodic) to each cut-off voltages (labeled on the figures) followed by DMC washing and drying. The spectrum of the film surface obtained after soaking (i.e. chemical reaction only) in the electrolyte for 24 h is also displayed for comparison. Note that when the electrodes were rinsed in DMC prior to *ex-situ* analysis, soluble surface species could be washed off. The chemically reacted film shows a dominant peak at 841 cm^{-1}, attributed to stretching modes of P^{5+}–F [12,15,16] probably from P–F-containing salts M^{n+}–PF (M = Li/Sn). Since Li^+ ions are likely solvated by EC and DMC solvents, the PF_6^- anions from $LiPF_6$ salt may actively interact with Sn metal at the interface, then, by electron transfer between them the bonding of Sn—(PF_x) can be formed. The presence of a trace of water impurity in electrolyte can cause the production of PF_5 by $LiPF_6 + H_2O \rightarrow PF_5 + LiF$, $PF_5 + H_2O \rightarrow HF + PF_3O$ [17]. Since not only PF_5 but also PF_3O are strong Lewis acids, the electron transfer from Sn to PF_5 and PF_3O just by contact can occur forming Sn–PF_5 or Sn–PF_3O precipitates. Also HF can possibly attack the surface of Sn forming SnF_2 or SnF_4. However, the IR features of Sn–F as well as LiF are reported to be below 600 cm^{-1} [18], thus, not detectable in the mid IR (700–4000 cm^{-1}) region that we used. Weak features of CH_3CH_2– (2970–2800 cm^{-1}) alkyl group and C=O (~1604 cm^{-1}) of carboxylate metal salt group are observed, indicating low amounted organic species produced.

The peak due to P–F group near 830–840 cm^{-1} remained as dominant on all the films regardless of cut-off voltages of charge and discharge processes. This indicates that PF-containing species is the major component in the surface layer. Fig. 2a and b show that charged and cycled film electrodes have the appearance of additional dominant peak near 730–740 cm^{-1}, attributable to the stretching mode of P^{3+}–F, consistent with other literature [15]. Electrochemical process seems to cause the partial reduction of P atom in the PF-containing species.

In contrast to the chemically reacted film, the films charged till 1.0 V did not show clear features from organics. This ensures that at the high voltage region mostly the PF_6^- anions participate in the interfacial reactions with Sn. When charging below 0.63 V, the film surface showed weaker IR features of alkyl group (2970–2800 cm^{-1}) than the chemically reacted film. However, the peak at 1535 cm^{-1}, attributed to C=O of carboxylate metal salts, became stronger, and a new weak peak near 1624 cm^{-1} and a shoulder at 1580 cm^{-1} appeared. There are several types of bonding for metal–carboxylate salt, and they show the strong IR features of asymmetric and symmetric stretching modes of C–O at slightly different frequency region; bidentate and bridging (1610–1515, 1495–1315 cm^{-1}) and unidentate (1675–1575, 1420–1260 cm^{-1}) [15,16]. In this aspect, the film surface appears to include various carboxylate metal salts at different bonding types, but the strongest peak at 1535 cm^{-1} is indicative of the bidentate or bridging type salt to be dominant. The appearance of the organic species, which must be produced by the decomposition of EC and DMC solvents, is together with the presence of small peaks at ~1270 and ~1060 cm^{-1}, assignable to stretching modes of P=O and P–O–C group probably from –O=PF–O*R* (*R* = organics) organic phosphorus fluoride compounds [12,15,16,19]. Also shown is the new peak at 897 cm^{-1}, which is stronger along with C=O and alkyl groups, particularly when charging to 0.63 V and cycling. This peak may be attributable to the strong stretching mode of other type of P^{5+}–F bonding from newly formed surface species or P–CH_3 group that are shown together with the peaks near 1430–1380, 1330–1280 cm^{-1} from C–H deformation modes [15]. Thus, the new peak of P–F at 897 cm^{-1} is thought to come from –O–PF–(O)*R* group. We speculate that PF-containing inorganic species could be involved in the decomposition of organic solvents and produce such –O–PF–(O)*R* organic phosphorus-fluoride containing compounds.

The film after charged to 0.1 V showed relatively low peaks intensity of organic species, compared to those for the film after charged to 0.63 V and cycling. Deep charging to 0.1 V seems not allow organic species to adhere to the surface of Sn, but rather destroy them and wash off at some point, probably associated with mechanical particle cracking occurring during full alloying, as discussed in later section (Fig. 3e). Nevertheless, the bonding between Sn and PF-containing species remained undetached showing high peak intensities, despite of particle cracking occurred.

The film surface after cycling showed the same IR features to those charged to 0.63 V, except the enhancement of the peak at 897 cm^{-1} and organic features. The peak at 897 cm^{-1}, attributed to P–F and/or P–CH_3 group, was significantly grown at the expense of the peak at 830–840 cm^{-1}. This reflects that some of originally formed PF-containing inorganic salts is converted to other type of P–F that is included in organic phosphorus-fluoride containing compounds. Considering that organic species are destroyed upon deep charging but reproduced upon discharging to 1.0 V, the deep charge is believed to be the process of unstabilizing the organic surface layer.

The FTIR study for the 58 nm thick Sn/SS film electrode demonstrates that P–F containing inorganic salts are the first formed surface species by Sn electrode–electrolyte interfacial reactions at high voltage region above 1.0 V. Then, organic surface species are produced and precipitated around 0.6 V, which may be located on underlying or between PF-containing inorganic salt grains.

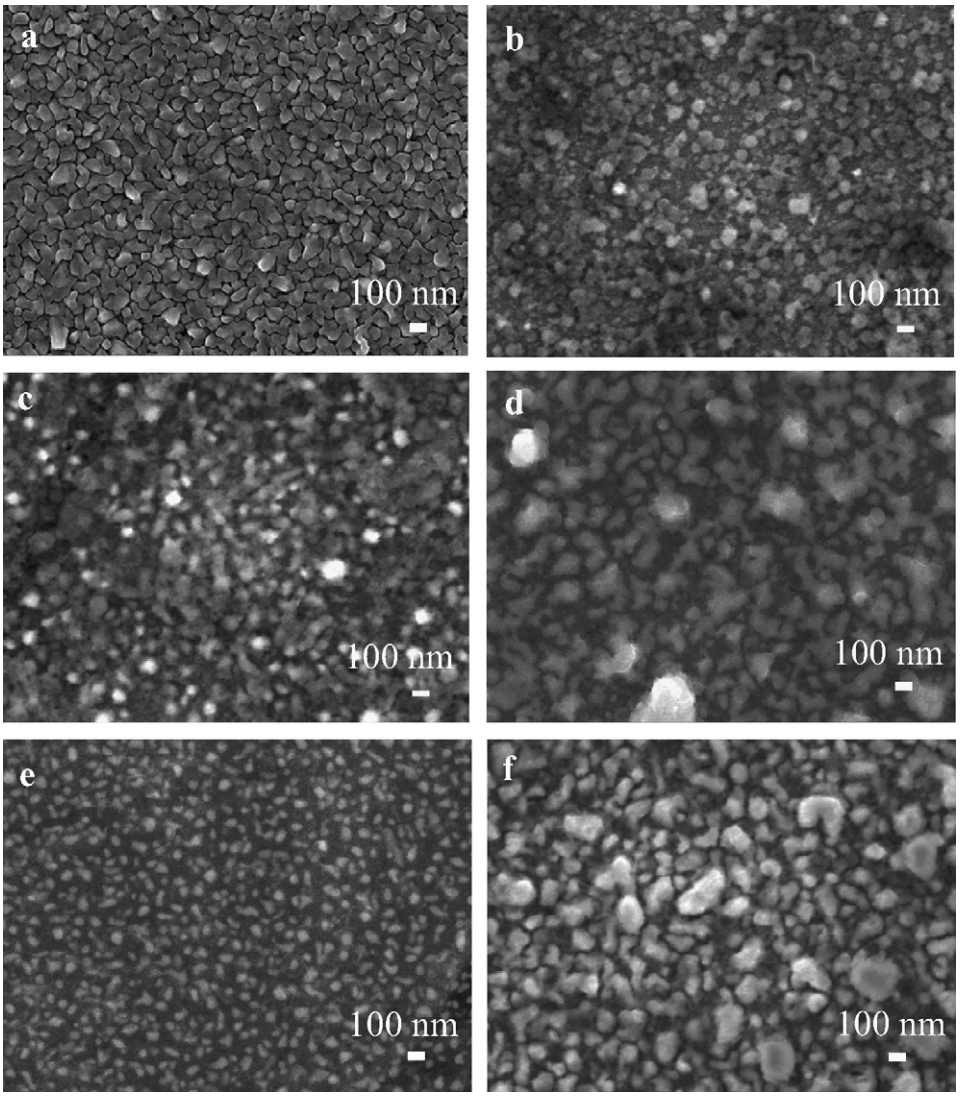

Fig. 3. SEM images of surface morphology for Sn/SS film electrodes (a) as-deposited and obtained after charging to (b) 1.5 V, (c) 1.0 V, (d) 0.63 V and (e) 0.1 V, and after (f) initial cycle at 0.1–1.0 V, followed by DMC washing and drying.

However, by deep charging, most organic surface species were destroyed and washed off, but reproduced upon the following discharging. If the dominant surface species of PF-containing inorganics covered the surface of Sn while not allowing the transport of lithium ions, their stable surface passivation of Sn should result in the loss of availability of active Sn for next cycling.

3.3. Film morphology changes after charging and cycling

The as-deposited 58 nm thick film of Sn was light grey and showed quite a dense and flat surface, where crystalline particles of 70–100 nm in size appear to be connected each other, as shown in Fig. 3a. Changes in the morphology of the Sn/SS film electrodes depending on charging and cycling were monitored with *ex-situ* SEM and displayed in Fig. 3b–f. The surface of charged and cycled film electrodes was grey to dark-brown. In Fig. 3b and c, with charging to 1.5–1.0 V surface particles seemed to begin separated from each other with the loss of particle crystallinity. IR data revealed that at this voltage region mostly PF-containing salts are present at the surface of Sn. With further charging to 0.63 V (Fig. 3d) particle size increased to 57–105 nm, probably due to alloying reaction followed by structural volume expansion, and tended to become amorphous. Recollecting the IR analysis results, this surface of Sn is covered with the mixture of P–F containing inorganic species and organics. With deep charge to 0.1 V (Fig. 3e) particle cracking into individual smaller grains of approximately 63 nm in average size was evident, consistent with earlier reported results [1,2]. Organic surface species must be destroyed and washed off at this stage. Particle cracking occurring as a consequence of Li–Sn alloying would certainly result in the reduced connectivity of particles but offer the increased active surface area that can further react with electrolyte. On the following discharge process to 1.0 V, Fig. 3f, an increase in particles size to 58–273 nm was observed and particles appeared back to crystalline. During this particle regrowth, some surface species and Li_xSn could possibly be incorporated into the inner space between grains and remained confined as disconnected. The SEM observation confirms that the most drastic particle morphology changes and surface roughening occur during deep charge and the subsequent discharge processes, resulting in the loss of particle connection. This should be related to the unstabilization of organic surface layer but the stable surface coverage by PF-containing inorganic species that seems not to play a SEI role. These are believed to be responsible for the large initial irreversible capacity loss of Sn electrode,

which predicts a continued deterioration of cyclability over next cycles.

4. Conclusions

Surface species produced on the thin film electrodes of Sn during initial cycling was characterized employing ATR FTIR spectroscopy. Both chemically and electrochemically the surface of the Sn was covered mainly by P–F containing species, indicating the active interfacial reactions between Sn and PF_6^- anions from lithium salt. Near 0.6 V the formation of organic surface species with the functionalities of carboxylate metal salt and alkyl groups began to be shown, which are involved in the formation of both organics only and organic phosphorus-fluoride compounds, due to the decomposition of organic solvents. However, the organic layer was found to be destroyed and washed off upon deep charging to 0.1 V, accompanied with significant particle cracking. Studies of the interfacial reaction behavior of Sn electrode suggest that appropriate electrolyte composition, which can initially construct a stable interfacial structure and protect the surface of Sn, is needed for improved cycling ability of Sn-based anode materials in lithium batteries.

Acknowledgments

This work was supported by the Korea Research Foundation Grant funded by the Korean Government (MOEHRD, Basic Research Promotion Fund, KRF-2006-531-D00001). The authors thank Techno Semichem for providing electrolytes and Woo-Chul Shin for his help with experiment.

References

[1] I. Rom, M. Wachtler, I. Papst, M. Schmied, J.O. Besenhard, F. Hofer, M. Winter, Solid State Ionics 143 (2001) 329.
[2] M. Winter, J.O. Besenhard, Electrochim. Acta 45 (1999) 31.
[3] K.-F. Chiu, H.C. Lin, K.M. Lin, T.Y. Lin, D.T. Shieh, J. Electrochem. Soc. 153 (2006) A1038.
[4] M. Inaba, T. Uno, A. Tasaka, J. Power Sources 146 (2005) 473.
[5] S.D. Beattie, T. Hatchard, A. Bonakdarpour, K.C. Hewitt, J.R. Dahn, J. Electrochem. Soc. 150 (2003) A701.
[6] S.-W. Song, R.P. Reade, E.J. Cairns, J.T. Vaughey, M.M. Thackeray, K.A. Striebel, J. Electrochem. Soc. 151 (2004) A1012.
[7] S.-W. Song, R.P. Reade, R. Kostecki, K.A. Striebel, J. Electrochem. Soc. 153 (2006) A12.
[8] S.-W. Song, S.-W. Baek, ECS Trans. 11 (2008) 71.
[9] G.V. Zhuang, P.N. Ross Jr., Electrochem. Solid-State Lett. 6 (2003) A136.
[10] K. Xu, Chem. Rev. 104 (2004) 4303.
[11] H. Bryngelsson, M. Stjerndahl, T. Gustafsson, K. Edström, J. Power Sources 174 (2007) 970.
[12] R. Aroca, M. Nazri, G.A. Nazri, A.J. Camargo, M. Trsic, J. Solution Chem. 29 (2000) 16.
[13] G.V. Zhuang, K. Xu, H. Yang, T.R. Jow, P.N. Ross Jr., J. Phys. Chem. B 109 (2005) 17567.
[14] S.V. Compton, D.A.C. Compton, Practical Sampling Techniques for Infrared Analysis, P.B. Coleman (Ed.), CRC Press, Boca Raton, FL, 1993.
[15] G. Socrates, Infrared Characteristic Group Frequencies; Tables and Charts, 2nd ed., John Wiley & Sons, 1994.
[16] N.B. Colthup, L.H. Daly, S.E. Wiberley, Introduction to Infrared and Raman Spectroscopy, 3rd ed., Academic Press, 1990.
[17] D. Aubarch, B. Markovsky, A. Shechter, Y. Ein-Eli, J. Electrochem. Soc. 143 (1996) 3809.
[18] K. Kanamura, H. Tamura, Z. Takehara, J. Electroanal. Chem. 142 (1995) 340.
[19] H. Yang, G.V. Zhuang, P.N. Ross Jr., J. Power Sources 161 (2006) 573.